

Article

Microstructure and Properties of Hybrid Laser Arc Welded Joints (Laser Beam-MAG) in Thermo-Mechanical Control Processed S700MC Steel

Jacek Górká ^{1,*}  and **Sebastian Stano** ²¹ Welding Department, Silesian University of Technology, Konarskiego 18A, 44-100 Gliwice, Poland² Welding Institute in Gliwice, Bl. Czesława 16-18, 44-100 Gliwice, Poland; sebastian.stano@is.gliwice.pl

* Correspondence: jacek.gorka@polsl.pl; Tel.: +48-32-237-1445

Received: 27 December 2017; Accepted: 9 February 2018; Published: 15 February 2018

Abstract: The article presents the microstructure and properties of joints welded using the Hybrid Laser Arc Welding (HLAW) method laser beam-Metal Active Gas (MAG). The joints were made of 10-mm-thick steel S700MC subjected to the Thermo-Mechanical Control Process (TMCP) and characterised by a high yield point. In addition, the welding process involved the use of solid wire GMn4Ni1.5CrMo having a diameter of 1.2 mm. Non-destructive tests involving the joints made it possible to classify the joints as representing quality level B in accordance with the ISO 12932 standard. Destructive tests of the joints revealed that the joints were characterised by tensile strength similar to that of the base material. The hybrid welding (laser beam-MAG) of steel S700MC enabled the obtainment of good plastic properties of welded joints. In each area of the welded joints, the toughness values satisfied the criteria related to the minimum allowed toughness value. Tests involving the use of a transmission electron microscope and performed in the weld area revealed the decay of the precipitation hardening effect (i.e., the lack of precipitates having a size of several nm) and the presence of coagulated titanium-niobium precipitates having a size of 100 nm, restricting the growth of recrystallised austenite grains, as well as of spherical stable TiO precipitates (200 nm) responsible for the nucleation of ferrite inside austenite grains (significantly improving the plastic properties of joints). The tests demonstrated that it is possible to make welded joints satisfying quality-related requirements referred to in ISO 15614-14.

Keywords: steel S700MC; hybrid welding; HLAW; laser beam; MAG

1. Introduction

The use of advanced technologies in metallurgical processing as well as a new look at the significance and the role of alloying elements used in steels have enabled the fabrication of various groups of steels characterised by vast ranges of mechanical and plastic properties [1]. The development of new steel grades, particularly high-strength low alloys (HSLA) having ferritic, ferritic-pearlitic, ferritic-bainitic, bainitic, or tempered martensitic structures, has made it possible to significantly reduce the weight of structural elements and that of entire structures [2–4]. The reduction of thicknesses of steels manufactured in thermo-mechanical control processes (TMCP) (dictated by the needs of the automotive, ship-building, and petroleum industries) without compromising previously obtained performance characteristics has made it possible to achieve significant savings resulting from lower material processing and transport-related costs [5–11]. Advanced TMCP steels must satisfy not only strength-related but also environmental and social criteria [12]. In the case of the arc welding and laser welding of thermomechanically rolled steels, joints with insufficient impact strength are obtained, but these deficiencies can be eliminated during the hybrid welding process [13–15]. During welding, the material's microstructure, which provides high strength and plastic properties and is achieved by

thermo-mechanical rolling, is destroyed. In weld metal, the structure of cast metal with properties are based on the used welding method (welding parameters) and additional material. Therefore, there is a need for the assessment of the welding method and parameters' impact on welded joints from steels, which parameters are a result of TMCP properties, especially when unconventional heat sources, such as a laser or laser-arc hybrids, are used [16–19].

The development of the above-named steels entails research works concerning various technologies enabling the joining of such steels [20–22]. Increasingly often, metals and their alloys are joined using highly efficient welding processes enabling the obtainment of high-quality welded joints accompanied by high joining process efficiency and less labour. The above-presented approach has resulted in the improvement of existing welding methods and, among other things, in the development of hybrid welding (in the late 1990s). However, only recently has the hybrid welding process seen growing popularity in, e.g., the shipbuilding or automotive industries, and it is gradually replacing laser and arc welding.

The hybrid laser arc welding (HLAW) technology combines two conventional welding methods. This process involves the simultaneous use of a heat source in the form of a laser radiation beam and an electric arc. According to the PN-EN ISO 15614-14 standard, a welding process can be referred to as hybrid where two coupled heat sources are used to form one common weld pool (Figure 1). The combination of two independent welding methods into one hybrid process results in the synergic effect of two heat sources. Consequently, the hybrid welding process is characterised by advantages typical of both methods. In addition, the above-presented combination reduces or eliminates limitations and disadvantages related to the use of only one heat source. Controversially, the beginning of the development of the hybrid technology (combining two independent heat sources) in welding engineering is seen by many as the announcement (in 1972) made by a group of engineers from the Philips Research Laboratory, Eindhoven, Holland (led by W.G. Essers and A. C. Liefkens) concerning the development of a new torch combining functions of plasma welding (PAW) and Gas Metal Arc Welding (GMAW). Initial attempts involving the combination of the laser method with the arc process were conducted at the Imperial College in London in the 1970s. A group of scientists supervised by William Steen demonstrated unquestionable advantages resulting from the combination of a plasma arc with a CO₂ laser beam. The welding rate increased by 50–100%, whereas the penetration depth increased by 20% when compared with that obtained using one heat source, i.e., a laser beam. The process of hybrid welding can involve the use of two independent heat sources with two independent technological heads. However, the foregoing requires precise positioning and the use of a simple system enabling the synchronised activation of both heat sources. In addition, it is possible to use special heads dedicated to the hybrid process that ensure the appropriate positioning of the two heat sources. In the HLAW, method it is possible to use nearly any industrial laser, yet the recent significant development of solid-state lasers (disc and fibre lasers) has made them the most popular sources of laser radiation in the hybrid method. In addition, a plasma cloud formed during the hybrid-welding process is more transparent for the electromagnetic wave emitted by the above-named lasers (approximately 1 μm), nearly entirely regardless of the type of shielding gas used in the arc method. Arc methods usually used in the HLAW method are those where the electrode is simultaneously filler metal fed to the welding area in a continuous manner (Metal Inert Gas (MIG), Metal Active Gas (MAG)). The filler metal makes it possible to adjust the chemical composition of the weld through supplying appropriate alloying elements to the weld pool and ensures the proper course of the welding process when a gap between joined elements is present (in terms of laser welding, there should be no gap between elements to be joined). The laser beam enables the obtainment of deep penetration using low linear energy, stabilises the arc, and improves the thermal efficiency of the process. The electrode wire ensures the complete filling of the weld groove gap and the formation of excess weld metal. The process of hybrid welding can be particularly useful in large-size industrial-scale production, primarily because of a higher acceptable tolerance when preparing the elements to be welded, the possibility of joining sheets in one run, and a lower

accuracy when positioning the sheets to be joined [23–31]. HLAW is a relatively new welding process which causes specific thermal conditions that result in a change of the crystallization mode and precipitation type and size in a welded joint. The aforementioned conditions have a substantial impact on the properties of thermo-mechanically rolled steel joints. Determination of HLAW welded joints' properties enables the application of contemporary, highly efficient welding technologies in an industrial environment. Industrial demand for research in the field of joining contemporary steels with recent welding processes was the basis for collaboration between the Silesian University of Technology and the Welding Institute.

In this study, the welding of novel hot-rolled 700 MPa tensile strength Nb-Ti-V microalloyed steels of 10 mm thickness was carried out by HLAW. The joint microstructure, hardness, strength, and impact toughness were examined, and face and root bend and radiographic tests were performed.

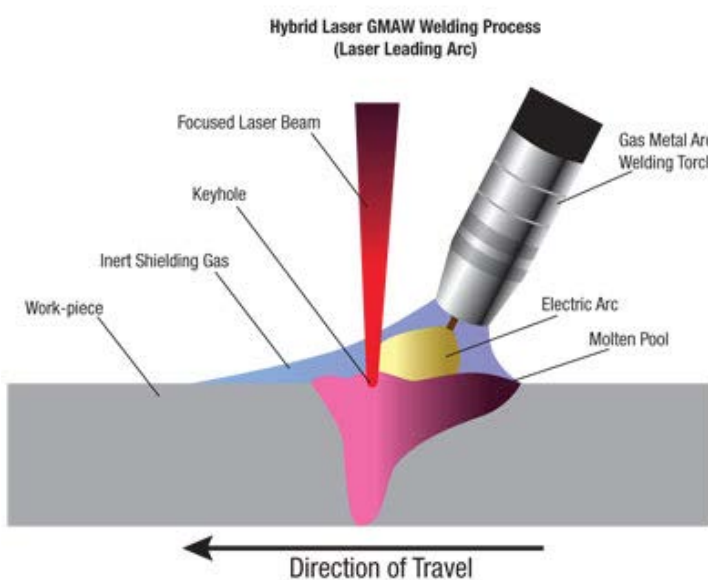


Figure 1. Schematic diagram of the hybrid welding process [26].

2. Experimental Section

The research-related tests aimed to identify the properties of butt hybrid welded (laser beam-MAG) joints made of 10-mm-thick steel S700MC using a copper strip and solid wire GMn4Ni1.5CrMo having a diameter of 1.2 mm. The chemical composition and the properties of the steel and weld deposit are presented in Tables 1 and 2, whereas the steel microstructure is presented in Figure 2.

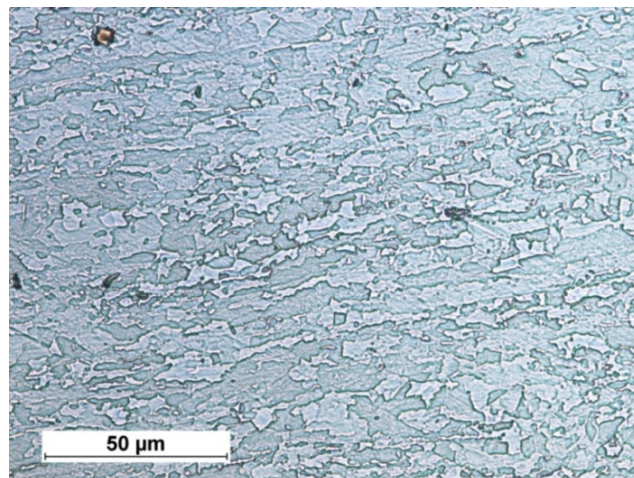
Table 1. The real chemical composition performed using Optical Emission Spectroscopy (OES) and the mechanical properties of the original S700MC steel material.

Chemical Composition, wt %												
C	Si	Mn	P	S	Al _{tot}	Nb	V	Ti	B	Mo.	Ce **	
0.056	0.16	1.18	0.01	0.005	0.027	0.044	0.006	0.12	0.002	0.0150	0.33	
Mechanical Properties												
Tensile Strength Rm, MPa			Yield Point Re, MPa			Elongation A ₅ , %			Hardness HV		Impact strength, J/cm ² (−20 °C)	
822			768			19			280		135	

* Total amount of Nb, V, and Ti should amount to a maximum of 0.22%. ** Ce: carbon equivalent.

Table 2. Chemical composition and mechanical properties of filler metal GMn4Ni1.5CrMo.

Chemical Composition, wt %						
C	Mn	Si	Cr	Ni	Mo	Ti
0.1	1.8	0.7	0.3	2.0	0.55	0.07
Mechanical Properties						
Tensile Strength R_m , MPa	Yield Point R_e , MPa		Elongation A_5 , %	Impact Strength, J/cm ² (-40°C)		
900	810		18	55		

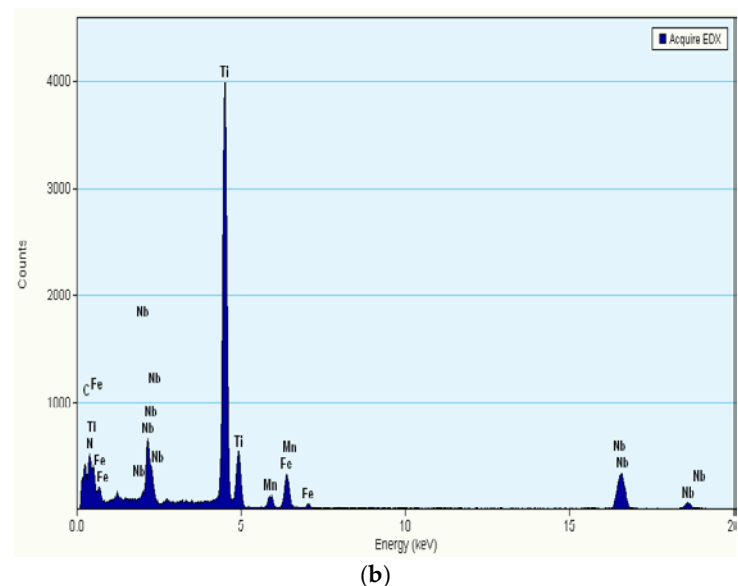
**Figure 2.** Microstructure of bainitic-ferritic steel S700MC with visible effects of plastic deformation.

The tests of thin foils performed using a transmission electron microscope revealed that the hardening of steel S700MC was primarily caused by dispersive $(\text{Ti},\text{Nb})(\text{C},\text{N})$ -type precipitates (a few nm in size) formed in the steel ferrite during cooling (Figure 3). The growth of recrystallised austenite grains in the steel was reduced by spherical $(\text{Nb},\text{Ti})\text{C}$ and $(\text{Ti},\text{Nb})(\text{C},\text{N})$ carbide precipitates having diameters of between 10 and 50 nm (Figure 4).

Element	Mass Concentration, %	Atomic Concentration, %
N K	10.77	32.72
Ti K	56.27	49.96
Mn K	1.74	1.34
Fe K	5.48	4.18
Nb (K)	25.72	11.77

(a)

Figure 3. Cont.



(b)

Figure 3. Precipitation of carbonitride $(\text{Ti},\text{Nb})(\text{C},\text{N})$ with numerous small dispersive precipitates corresponding to the hardening of the steel. (a) recipitation of carbonitride $(\text{Ti},\text{Nb})(\text{C},\text{N})$; (b) large particle-related EDX spectrum.

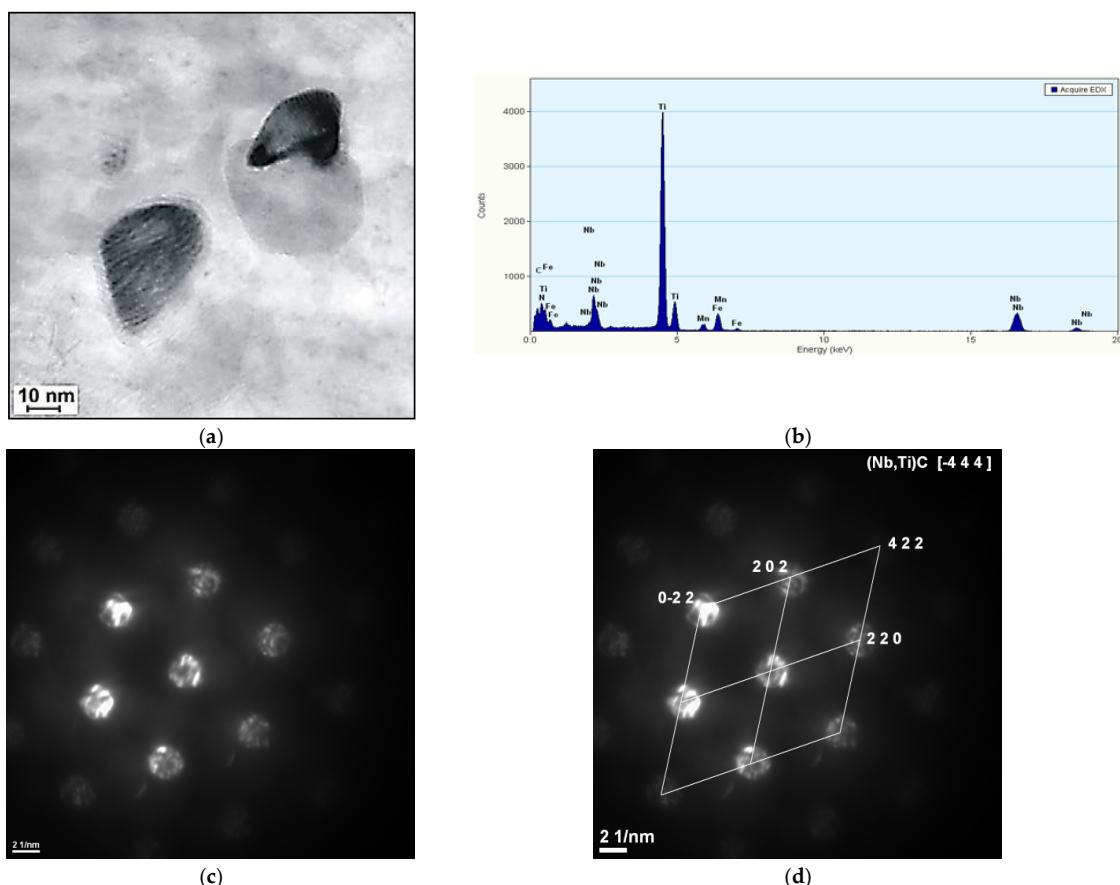


Figure 4. Dispersive precipitation of carbides $(\text{Ti},\text{Nb})\text{C}$ in S700MC steel limiting the growth of recrystallized austenite grains. (a) dispersive precipitation of carbides $(\text{Ti},\text{Nb})\text{C}$; (b) EDX spectrum; (c) diffraction pattern; (d) diffraction pattern solution.

2.1. Welding Process

The welded joints were made at Welding Institute in Gliwice using a robotic station (Figure 5). The tests were performed using a TruLaser Robot (TRUMPF, Stuttgart, Germany) 5120 cell-equipped with a TruDisk 12002 disc laser (TRUMPF, Stuttgart, Germany) having a power of 12,000 W (wavelength $\lambda = 1030$ nm) and an EWM Phoenix 452 RC PULS (EWM AG, Mündersbach, Germany) synergic power source. The hybrid welding head (laser beam-MAG) was fixed on the robot's wrist. The focal length of the laser optics collimator was $f_c = 200$ mm, whereas the focal length of the focusing lens amounted to $f_{foc} = 400$ mm. The diameter of the optical fibre supplying energy from the laser to the robot was $d_{fiber} = 0.4$ mm. The above-presented arrangement of the optics made it possible to obtain a laser beam focus diameter $d_{foc} = 0.8$ mm (Figure 6). The electrode extension was $l = 18$ mm. The shielding gas used in the tests was mixture M21 (18% CO₂ + 82% Ar), whereas the gas flow rate amounted to 18 dm³/min. The filler metal was solid wire GMn4Ni1.5CrMo having a diameter of 1.2 mm. The welding process was carried out in one pass. The electrode was inclined in relation to the welded surface at angle $\alpha = 65^\circ$, whereas the distance between the electrode tip and the laser beam was $a = 2$ mm (Figure 6). The parameters used when making the joint (adjusted on the basis of preliminary tests [32,33]) are presented in Table 3.

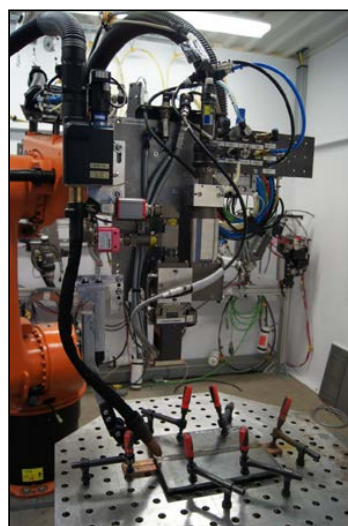


Figure 5. Hybrid welding station (laser beam-Metal Active Gas (MAG)).

Table 3. Parameters of the hybrid welding of 10-mm-thick steel S700MC.

Pre-Weld Metal Preparation			Welding Sequence			
Beam Power, W	Welding Rate, m/min	Wire Feeding Rate, m/min	Welding Current, A	Arc Voltage, V	Width of the Gap, mm	
5000	0.7	8	250	22	0.7	

Shielding gas: C18 ferromix; filler metal wire: GMn4Ni1.5CrMo having a diameter of 1.2 mm; welding performed using a copper strip: a rectangular groove; dimension of welded joints: 350 mm × 150 mm × 10 mm; fixing with metalwork clamps; a copper washer on the side of the weld ridge; positioning of the laser beam in the axis of the welding groove.

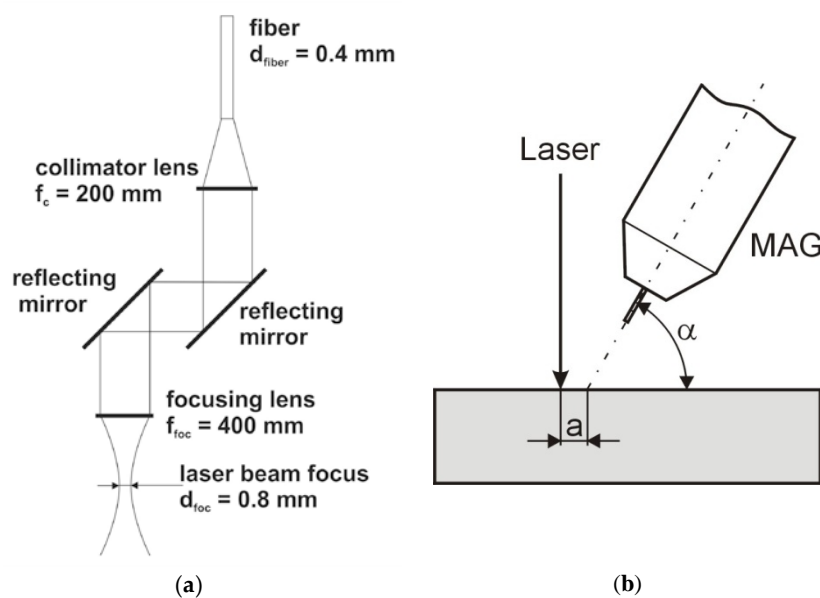


Figure 6. Diagram of the laser optical system and the position of the laser beam and electric arc in the hybrid technology. (a) the laser optical system; (b) position of the laser beam and electric arc.

2.2. Tests of Welded Joints

The test welded joint was subjected to the following non-destructive tests:

- visual tests performed on the basis of the requirements specified in the PN-EN ISO 17637:2011 standard;
- magnetic particle tests performed following the guidelines referred to in the PN-EN ISO 3059:2005, PN-EN ISO 9934-2:2003, and PN-EN ISO 9934-3:2003 standards. The necessary contrast was obtained using white contrast paint MR 72. The tests were performed using magnetic powder suspension MR 76S (MR International, Fränkisch-Crumbach, Germany) and a yoke electromagnet;
- radiographic tests based on the PN-EN 1435 standard performed using a CERAM 235 X-ray tube (Balteau NDT, Hermalle-sous-argenteau, Belgium) with the X-ray beam having a diameter $d = 2$ mm, a voltage $U = 180$ kV, a current $I = 3$ mA, and intensifying screens OW of -0.15 mm. The test results were recorded using an AGFA C5 photographic plate with an exposure time $t = 2.3$ min and a focal length $f = 700$ mm. Images were assessed using a 13FEEN wire-type image quality indicator.

Following the non-destructive tests, the welded joint was subjected to the following destructive tests:

- tensile tests performed in accordance with PN-EN ISO 6892-1:2010 using a ZWICK/ROELL Z 330RED (Zwick Roell, Ulm, Germany) testing machine and specimens sampled in accordance with PN-EN ISO 4136:2011 (dimensions of the sample: $300\text{ mm} \times 35\text{ mm} \times 10\text{ mm}$);
- a face bend test of the butt weld (FBB) and a root bend test of the butt weld (RBB) performed in accordance with the PN-EN ISO 5173:2010 standard (dimensions of the sample: $300\text{ mm} \times 20\text{ mm} \times 10\text{ mm}$). The bend tests were performed using a ZWICK/ROELL Z 330RED testing machine (Zwick Roell, Ulm, Germany) with an additional module enabling the performance of bend tests involving the use of a bending mandrel having a diameter of 30 mm. The distance between the rollers was set at 60 mm. To identify the position of the weld axis, the faces of the specimens were etched using Adler's reagent;
- impact strength tests performed in accordance with PN-EN ISO 148-1:2010 using specimens with the V-notch and a ZWICK/ROELL RKP 450 impact testing machine (Zwick Roell, Ulm, Germany). The tests were conducted at a temperature of -30°C (due to industrial requirements). Because of

the thickness of the plates being welded (10 mm) and the necessity of performing a preparatory mechanical treatment, the specimens were reduced in cross-section to 7.5 mm. The samples were extracted from the base metal, the heat-affected zone (HAZ), and the FL (fusion line), and the specimens were etched using Nital;

- macroscopic metallographic tests performed using an Olympus SZX9 light stereoscopic microscope (Olympus, Tokyo, Japan); the test specimens were etched using Adler's reagent (CHMES, Poznań, Poland);
- microscopic metallographic tests performed using a NIKON ECLIPSE MA100 light microscope (Nikon, Tokyo, Japan); the test specimens were etched using Nital;
- hardness measurements performed using a Vickers 401MVD hardness testing machine (Wilson Wolpert, Norwood, Massachusetts, USA) and a load of 1 kg;
- X-ray phase analysis performed using an X'Pert PRO diffractometer and an X'Celerator strip detector (PANalytical, Almelo, The Netherlands);
- tests of thin foils performed using a Titan 80–300 kV (FEI) high-resolution scanning transmission electron microscope (HR S/TEM, Thermo Fisher Scientific, Waltham, MA, USA) provided with an XEGF electron gun with the Schottky field emission characterised by enhanced brightness.

Samples for destructive testing were prepared by machining.

3. Results and Discussion

The visual tests and the magnetic particle tests of the welded joint did not reveal surface-breaking welding imperfections, such as cracks, porosity, incomplete fusion, or a lack of penetration (Figure 7). The radiographic tests did not reveal the presence of internal welding imperfections. The welded joint satisfied the requirements related to quality level B according to ISO 12932. The macroscopic metallographic tests did not reveal the presence of welding imperfections in the weld and HAZ (Figure 8). Excess penetration in the weld root was related to the shape and dimensions of the copper strip used during welding.

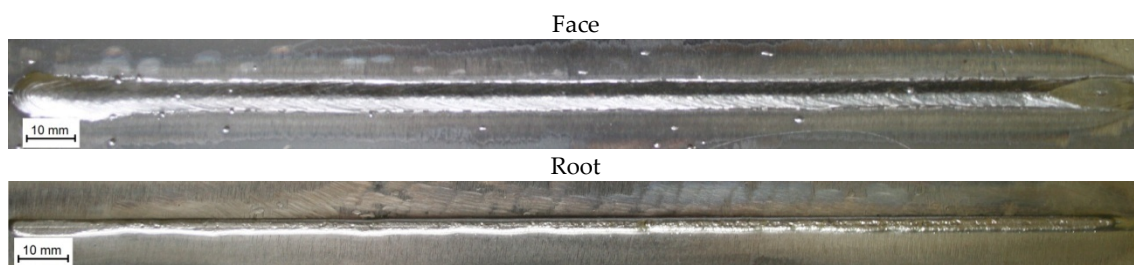


Figure 7. The face and the root of the hybrid welded joint (laser beam-MAG) in steel S700MC.

The microscopic metallographic tests revealed a bainitic-ferritic microstructure in the weld area. The heat-affected zone (HAZ) was characterised by variably sized grains, which could be ascribed to a significant heat input during the hybrid welding process (Figure 9). In addition, the microscopic tests revealed the probability of nitride precipitates' presence in the HAZ and in the base material; this is evidenced by their distinctive sharp shape (Figure 10). HLAW welding is characterized by relatively short cooling times $t_{8/5}$, which leads to the formation of martensite in the HAZ. However, as it is low-carbon martensite, it has no negative impact on plastic properties. In specific region of the HAZ with an increase of distance to the fusion line, ferrite content is increasing in lieu of bainite.

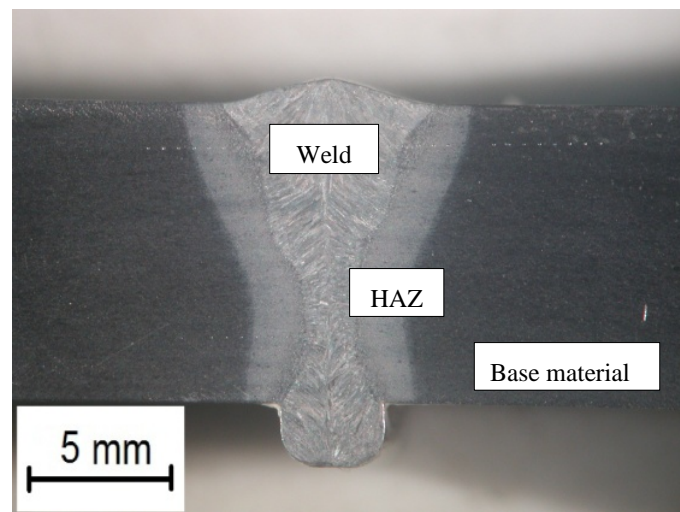


Figure 8. Macrostructure of the hybrid welded joint (laser beam-MAG) made in steel S700MC. HAZ: heat-affected zone.

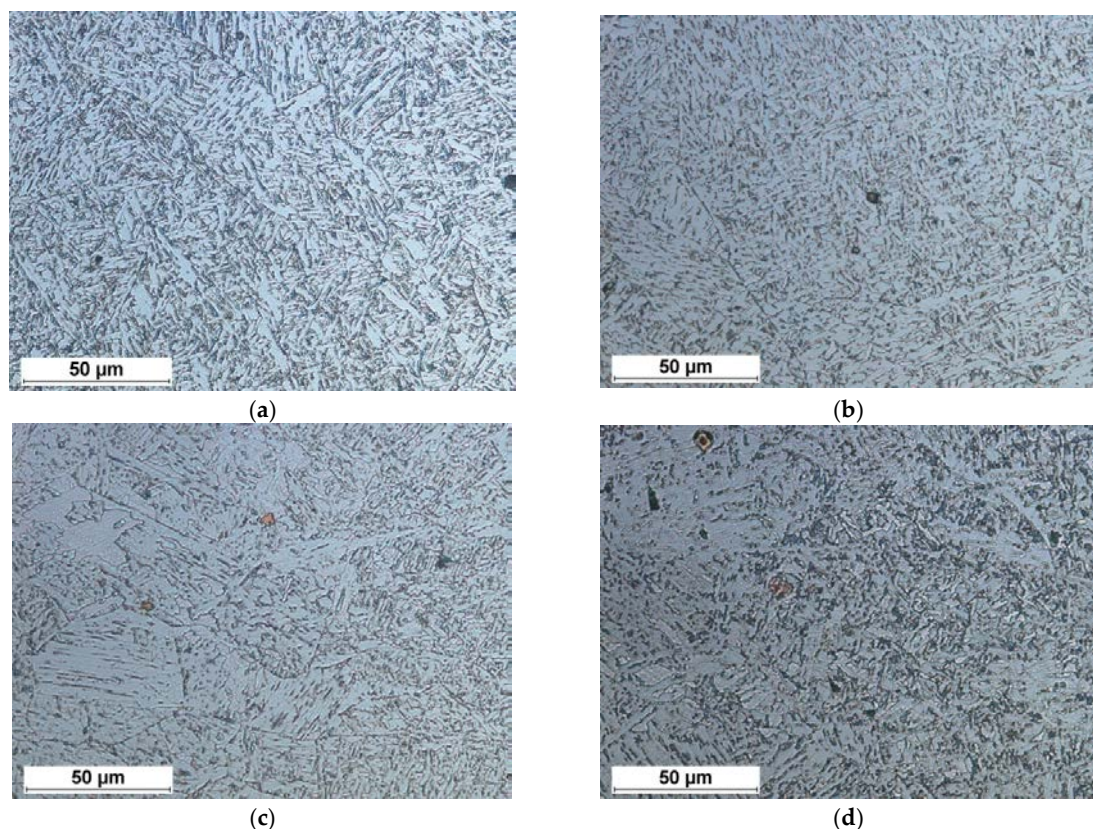


Figure 9. Cont.

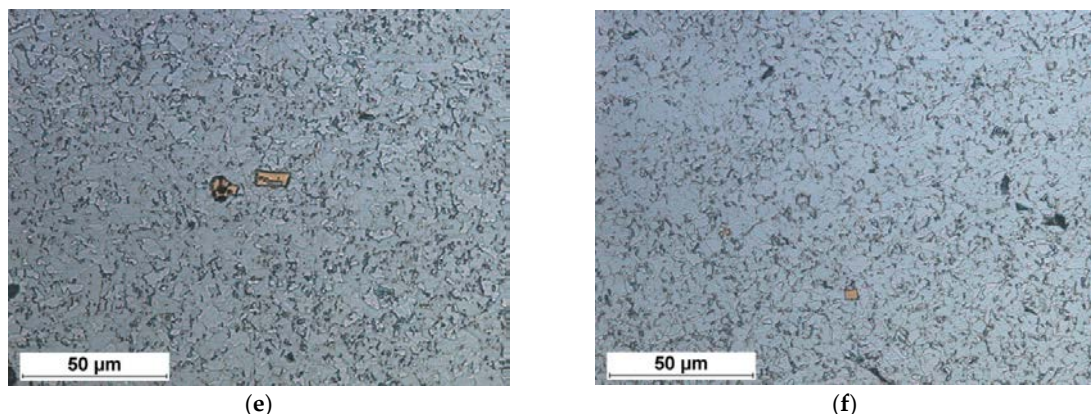


Figure 9. Microstructure of the hybrid welded joint (laser beam-MAG). (a) microstructure of the upper part of the weld; (b) microstructure of the lower part of the weld; (c) microstructure of the upper part of the fusion line; (d) microstructure of the lower part of the fusion line; (e) microstructure of the coarse-grained part of the HAZ; (f) microstructure of the fine-grained part of the HAZ.

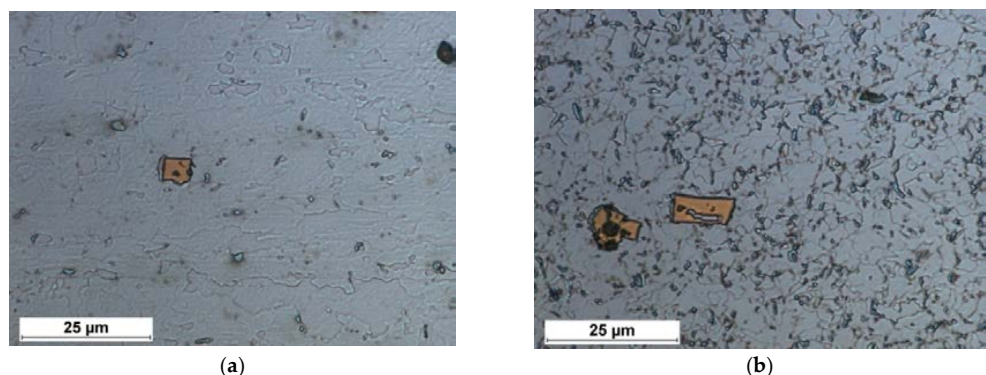


Figure 10. Nitride precipitates in the hybrid welded joint (laser-MAG) made of S700MC steel. (a) base material; (b) HAZ.

The analysis of the destructive test results of the hybrid butt welded joint (laser beam-MAG) revealed that the test joint satisfied the requirements of the ISO 15614-14 standard (Table 4). The hybrid welding process (laser beam-MAG) resulted in a slight decrease in tensile strength (to approximately 790 MPa) in relation to the hardness of the base material (820 MPa). The rupture took place in the HAZ (an area of slight grain growth). The above-named decrease in tensile strength was connected with the loss of properties obtained by steel S700MC through the thermo-mechanical control process. This is mainly related to the increase in the proportion of ferrite in the structure and the grain growth in this area. The bend test resulted in a bend angle of 180°, both during bending on the face and root side, which demonstrated the high plastic properties of the joint. The impact strength test performed at a temperature of -30 °C revealed satisfactory toughness values in the weld, fusion line, and the HAZ. In the weld area, the toughness amounted to 89 J/cm². In the fusion line area, the toughness decreased to approximately 50 J/cm². In the HAZ, the toughness amounted to approximately 40 J/cm², (samples for impact tests were cut across the welded joint). The toughness of the base material amounted to 50 J/cm².

Table 4. Strength and plastic properties of the hybrid weld joint (laser beam-MAG) made of S700MC steel.

Tensile Strength *		Bending *, Bend Angle, °		Impact Strength KCV **, J/cm ² (Test Temperature –30 °C)		
R _m , MPa	Area of Rupture	Face	Root	Weld	FL	HAZ
790	HAZ	180	180	89	51	42

FL: Fusion line; * average result of two measurements; ** average result of three measurements.

The hardness measurements concerning the hybrid welded joints made in steel S700MC revealed that the lowest hardness was characteristic of the heat-affected zone and amounted to approximately 227 HV, whereas the highest hardness was that of the base material and amounted, on average, to 280 HV. The difference between the hardness of the base material and that of the HAZ amounted to approximately 20%. The hardness value in the upper part of the weld was similar to that of the base material (280 HV1) and was higher than the value measured in the lower part of the weld (by approximately 8%). The foregoing could be attributed to the fact that the upper part of the weld contained more alloying elements, increasing the hardenability (nickel, chromium) supplied along with the filler metal (Figure 11).

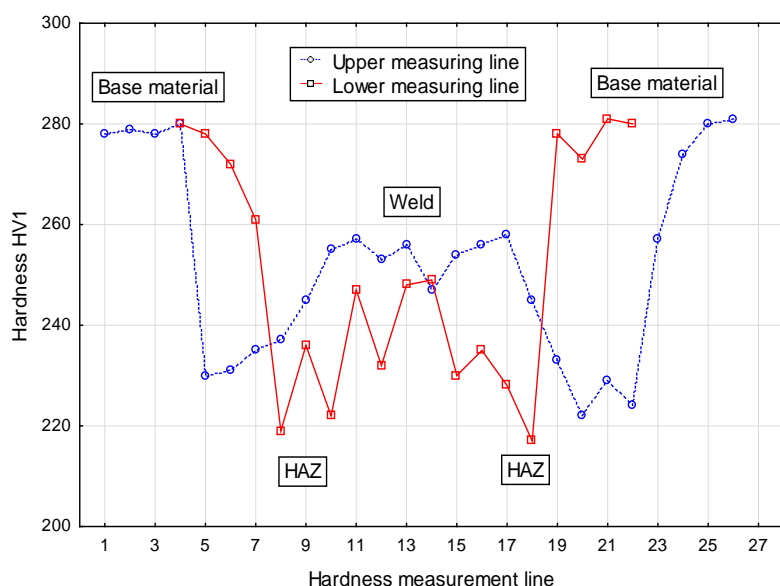


Figure 11. Hardness of the hybrid weld joint (laser beam-MAG) made of S700MC steel (position of measuring lines 2 mm from the top and bottom surface of the sheet).

The X-ray phase analysis revealed that the weld contained phase Fe α and a slight amount of phase Fe γ (Figure 12). The presence of phase Fe γ could be attributed to the presence of austenitic alloying elements, e.g., Ni or C, in the weld deposit. The analysis of the total intensity of X-radiation diffraction maxima from the lattice plane of phases Fe α and Fe γ of individual welded joints made it possible to determine that the content of retained austenite was restricted within the range of 3–6%.

The microscopic observations revealed that carbonitride precipitates (of several μm in size) in the weld area were dissolved entirely as a result of hybrid welding. The above-named observations were additionally confirmed by observations performed using the transmission electron microscope. The weld area was characterised by the decay of the precipitation hardening effect (lack of precipitates of several nm in size) and the presence of coagulated titanium-niobium precipitates of up to 500 nm (Figure 13), preventing the growth of recrystallised austenite and, consequently, improving the plastic properties of the weld. In addition, the weld area contained spherical and stable TiO₂.

precipitates (of 200 nm in size) responsible for the nucleation of ferrite inside austenite grains (Figure 14). The presence of the above-named ferrite translated into the high mechanical and plastic properties of the welded joints. This oxide is very stable even at high temperature and leads to ferrite formation inside coarse-grained HAZ grains.

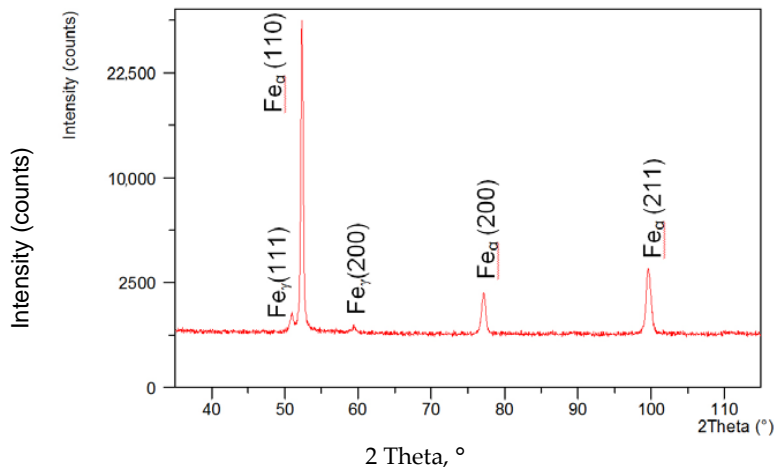


Figure 12. X-ray diffraction of the butt weld made in steel S700 MC.

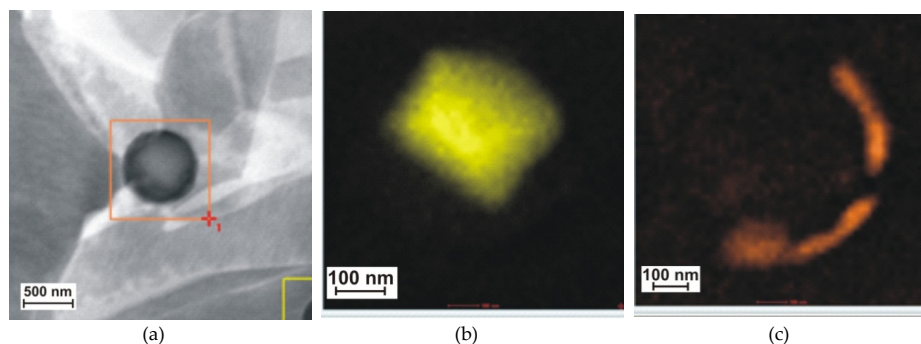


Figure 13. Titanium-niobium precipitates in the hybrid welded joint made of steel S700MC. (a) precipitate; (b) surface distribution of titanium; (c) surface distribution of niobium).

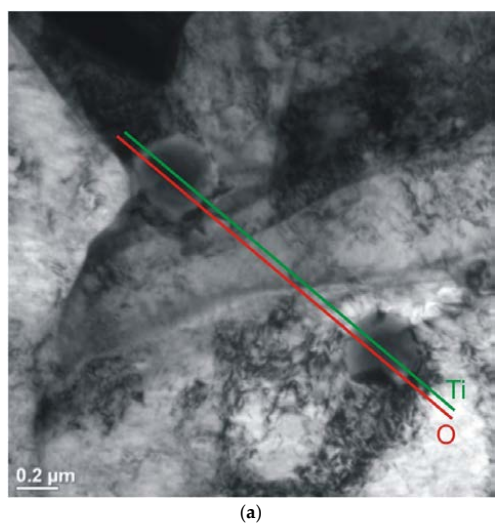


Figure 14. Cont.

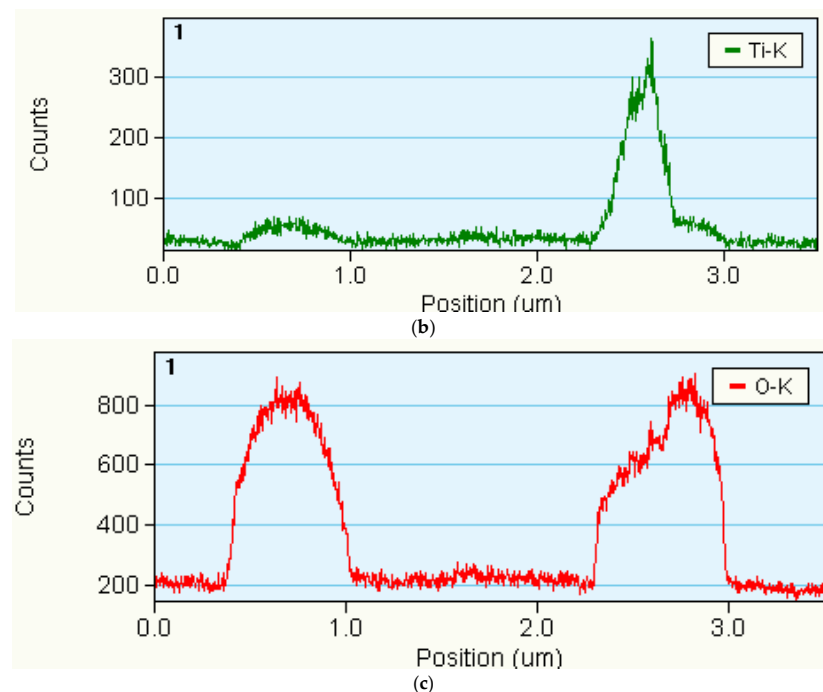


Figure 14. Spherical TiO precipitates in the hybrid welded joint made of steel S700MC. (a) precipitates; (b) linear analysis EDS of titanium concentration; (c) linear analysis EDS of oxygen concentration.

4. Conclusions

The tests of the hybrid welding (laser beam-MAG) of 10-mm-thick steel S700MC involving the use of a filler metal having the form of solid wire GMn4Ni1.5CrMo (1.2 mm in diameter) revealed the possibility of making welded joints satisfying the criteria formulated in the ISO 15614-14 standard. The test joints were characterised by a lack of welding imperfections as regards the shape, geometry, and discontinuity of the weld metal in the cross-section of the welded joint. The tensile strength of the welded joints was similar to that of the base material, whereas the plastic properties of the joints were satisfactory. The bend test performed both on the weld face and on the weld root side enabled the obtainment of a bend angle of 180° , whereas the toughness in the weld, fusion line, and in HAZ satisfied the criteria of the minimum yield point in relation to welded joints. The fusion line revealed a decrease in hardness, yet within a relatively narrow range and without compromising the operational properties of the welded joints. The microscopic tests of the welded joints revealed that the weld contained the typical bainitic-ferritic microstructure of dendritic nature. The heat-affected zone contained areas of variously sized grains, which was triggered by the thermal cycle effect. The HAZ and the base material revealed the presence of phases containing hardening microagents in the form of significant titanium nitride precipitates (indicated by their shape and the considerable content of titanium in the steel). The increase in the base material content in the weld was accompanied by the increase in the concentration of hardening microagents in the weld. The longer the time at which the material remained in the liquid state, the greater the amount of microagents which could dissolve in the matrix and re-precipitate (during cooling) or remain in the solution. The high temperature of the liquid metal pool could have resulted in the dissolution of even the most stable TiN particles. The cooling process did not provide appropriate conditions enabling the controlled re-precipitation of fine-dispersive carbides and carbonitrides (Ti_xNb) responsible for precipitation hardening. The welds made using the hybrid welding method were characterised by higher toughness resulting from the decay of the precipitation hardening effect (coagulation of precipitates) and the presence of spherical TiO precipitates responsible for the nucleation of ferrite inside austenite grains and, consequently, significantly improving the mechanical and plastic properties of the weld.

Acknowledgments: Work carried out as part of own research.

Author Contributions: Jacek Górká: assumptions, methodology, metallographic studies, analysis of test results, conclusions. Sebastian Stano: practical tests, optimization of welding parameters, destructive tests.

Conflicts of Interest: The authors declare no conflict of interest.

References

1. Flaxa, V.; Shaw, J. Material applications in ULSAB-AVC. *Steel Grips* **2003**, *1*, 255–261.
2. Opiela, M. Thermodynamic analysis of the precipitation of carbonitrides in microalloyed steels. *Mater. Tehnol.* **2015**, *49*, 395–401. [[CrossRef](#)]
3. Opiela, M. Elaboration of thermomechanical treatment conditions of Ti-V and Ti-Nb-V microalloyed forging steels. *Arch. Metall. Mater.* **2014**, *59*, 1181–1188. [[CrossRef](#)]
4. Grajcar, A. Thermodynamic analysis of precipitation processes in Nb-Ti-microalloyed Si-Al TRIP steel. *J. Therm. Anal. Calorim.* **2014**, *118*, 1011–1020. [[CrossRef](#)]
5. Mikia, C.; Homma, K.; Tominaga, T. High strength and high performance steels and their use in bridge structures. *J. Constr. Steel Res.* **2002**, *58*, 3–20. [[CrossRef](#)]
6. Lee, C.; Shin, H.; Park, K. Evaluation of high strength TMCP steel weld for use in cold regions. *J. Constr. Steel Res.* **2012**, *74*, 134–139. [[CrossRef](#)]
7. Ollilainen, V.; Hurmola, H.; Pontinen, H. Mechanical properties and machinability of a high-strength, medium-carbon, microalloyed steel. *J. Mater. Energy Syst.* **1984**, *5*, 222–232. [[CrossRef](#)]
8. Shipitsyn, S.; Babaskin, Y.; Kirchu, I.; Smolyakova, L.; Zolotar, N. Microalloyed steel for railroad wheels. *Steel Transl.* **2008**, *38*, 782–785. [[CrossRef](#)]
9. Rak, I.; Gliha, V.; Kocak, M. Weldability and toughness assessment of Ti-microalloyed offshore steel. *Metall. Mater. Trans.* **1997**, *28*, 199–206. [[CrossRef](#)]
10. Chang, K.; Lee, C.; Park, K.; Um, T. Experimental and numerical investigations on residual stresses in a multi-pass butt-welded high strength SM570-TMCP steel plate. *Int. J. Steel Struct.* **2011**, *11*, 315–324. [[CrossRef](#)]
11. Nishioka, K.; Ichikawa, K. Progress in termomechanical control of steel plates and their commercialization. *Sci. Technol. Adv. Mater.* **2012**, *13*, 023001. [[CrossRef](#)] [[PubMed](#)]
12. Grajcar, A.; Różański, M.; Kamińska, M.; Grzegorczyk, B. Effect of gas atmosphere on the non-metallic inclusions in laser-welded TRIP steel with Al and Si additions. *Mater. Tehnol.* **2016**, *50*, 945–950. [[CrossRef](#)]
13. Żuk, M.; Górká, J.; Czupryński, A.; Adamia, M. Properties and structure of the weld joints of quench and tempered 4330V steel. *Metalurgija* **2016**, *55*, 613–616.
14. Górká, J. Microstructure and properties of the high-temperature (HAZ) of thermo-mechanically treated S700MC high-yield-strength steel. *Mater. Tehnol./Mater. Technol.* **2016**, *50*, 617–621. [[CrossRef](#)]
15. Górká, J. Welding Thermal Cycle-Triggered Precipitation Processes in Steel S700MC Subjected to the Thermo-Mechanical Control Processing. *Arch. Metall. Mater.* **2017**, *62*, 331–336. [[CrossRef](#)]
16. Burdzik, R.; Węgrzyn, T.; Konieczny, Ł.; Lisiecki, A. Research on influence of fatigue metal damage of the inner race of bearing on vibration in different frequencies. *Arch. Metall. Mater.* **2014**, *59*, 1275–1281. [[CrossRef](#)]
17. Kurc-Lisiecka, A.; Piwnik, J.; Lisiecki, A. Laser welding of new grade of advanced high strength steel STRENX 1100 MC. *Arch. Metall. Mater.* **2017**, *62*, 1651–1657. [[CrossRef](#)]
18. Górká, J.; Janicki, D.; Fidali, M.; Jamrozik, W. Thermographic Assessment of the HAZ Properties and Structure of Thermomechanically Treated Steel. *Int. J. Thermophys.* **2017**, *38*, 183. [[CrossRef](#)]
19. Janicki, D.; Górká, J.; Kwaśny, W.; Gołombek, K.; Kondracki, M.; Żuk, M. Diode laser surface alloying of armor steel with tungsten carbide. *Arch. Metall. Mater.* **2017**, *62*, 473–481. [[CrossRef](#)]
20. Grajcar, A.; Matter, P.; Stano, S.; Wilk, Z.; Różański, M. Microstructure and hardness profiles of bifocal laser-welded DP-HSLA steel overlap joints. *J. Mater. Eng. Perform.* **2017**, *26*, 1920–1928. [[CrossRef](#)]
21. Grajcar, A.; Morawiec, M.; Różański, M.; Stano, S. Twin-spot laser welding of advanced high-strength multiphase microstructure steel. *Opt. Laser Technol.* **2017**, *92*, 52–61. [[CrossRef](#)]
22. Kubiak, M.; Piekarzka, W.; Stano, S.; Saternus, Z.; Domański, T. Numerical Prediction of Deformations in Laser Welded Sheets Made of X5CrNi18-10 Steel. *Arch. Metall. Mater.* **2015**, *60*, 1965–1972. [[CrossRef](#)]

23. Naito, Y.; Katayama, S.; Matsunawa, A. Keyhole behaviour and liquid flow in molten pool during laser-arc hybrid welding. In Proceedings of the International Congress on Laser Advanced Materials Processing (LAMP 2002), Osaka, Japan, 27–31 May 2002; Volume 4831, pp. 357–363.
24. Bagger, C.; Olsen, F. Comparison of plasma, metal inactive gas (MIG) and tungsten inactive gas (TIG) processes for laser hybrid welding. In Proceedings of the International Congress on Applications of Laser and Electro-Optics (ICALEO 2003), Jacksonville, FL, USA, 13–17 October 2003; pp. 11–20.
25. Orozco, N.J. Fully integrated hybrid-laser welding control process, Processes for Laser Hybrid Welding. In Proceedings of the International Congress on Applications of Laser and Electro-Optics (ICALEO 2003), Jacksonville, FL, USA, 13–17 October 2003; pp. 31–40.
26. Murakami, T.; Shin, M.H.; Nakata, K. Effect of welding direction on weld bead formation in high power fiber laser and MAG arc hybrid welding. *Trans. JWRI* **2010**, *39*, 175–177.
27. Banasiak, M.; Urbańczyk, M. Laser + MAG Hybrid Welding of Various Joints. *Biul. Inst. Spaw.* **2017**. [[CrossRef](#)]
28. Banasiak, M.; Urbańczyk, M. Laser + MAG Hybrid Welding of T-Joints. *Biul. Inst. Spaw.* **2017**. [[CrossRef](#)]
29. Banasiak, M.; Turyk, E.; Urbańczyk, M. Spawanie hybrydowe laser + MAG elementów urządzeń dźwigowych wykonanych ze stali ulepszonej cieplnie S960QL. *Prz. Spaw.* **2017**, *89*. [[CrossRef](#)]
30. Wang, X.-N.; Zhang, S.-H.; Zhou, J.; Zhang, M.; Chen, C.-J.; Misra, R.D.K. Effect of heat input on microstructure and properties of hybrid fiber laser-arc weld joints of the 800 MPa hot-rolled Nb-Ti-Mo microalloyed steels. *Opt. Lasers Eng.* **2017**, *91*, 86–96. [[CrossRef](#)]
31. Sun, Q.; Di, H.-S.; Li, J.-C.; Wu, B.-Q.; Misra, R.D.K. A comparative study of the microstructure and properties of 800MPa microalloyed C-Mn steel welded joints by laser and gas metal arc welding. *Mater. Sci. Eng. A* **2016**, *669*, 150–158. [[CrossRef](#)]
32. Górką, J. Właściwości i Struktura Złączów Stali Obrabianej Termomechanicznie o Wysokiej Granicy Plastyczności; Wydawnictwo Politechniki Śląskiej: Gliwice, Poland, 2013.
33. Górką, J.; Stano, S. The structure and properties of filler metal-free laser beam welded joints in steel S700MC subjected to TMCP. In *Laser Technology 2016: Progress and Applications of Lasers*; SPIE: Bellingham, WA, USA, 2016; Volume 10159, pp. 183–190.



© 2018 by the authors. Licensee MDPI, Basel, Switzerland. This article is an open access article distributed under the terms and conditions of the Creative Commons Attribution (CC BY) license (<http://creativecommons.org/licenses/by/4.0/>).